Low-temperature transport in ac-driven quantum dots in the Kondo regime

Rosa López,[1] Ramón Aguado,[2] Gloria Platero,[1] and Carlos Tejedor[3]
[1]*Teoría de la Materia Condensada, Instituto de Ciencia de Materiales (CSIC), Cantoblanco, 28049 Madrid, Spain*
[2]*Center for Materials Theory, Department of Physics and Astronomy, Rutgers University, Piscataway, New Jersey 08854-8019*
[3]*Departamento de Física Teórica de la Materia Condensada, Universidad Autónoma de Madrid, Cantoblanco, 28049 Madrid, Spain*
(Received 18 September 2000; revised manuscript received 14 February 2001; published 31 July 2001)

We present a fully nonequilibrium calculation of the low-temperature transport properties of a quantum dot in the Kondo regime when an ac potential is applied to the gate. We solve a time-dependent Anderson model with finite on-site Coulomb interaction. The interaction self-energy is calculated up to second order in perturbation theory in the on-site interaction, in the context of the Keldysh nonequilibrium technique, and the effect of the ac voltage is taken into account exactly for all ranges of ac frequencies and ac intensities. The obtained linear conductance and time-averaged density of states of the quantum dot evolve in a nontrivial way as a function of the ac frequency and ac intensity of the harmonic modulation.

DOI: 10.1103/PhysRevB.64.075319 PACS number(s): 73.40.Gk, 72.15.Qm, 85.35.Be, 73.50.Mx

I. INTRODUCTION

Recent experiments[1–3] showing Kondo behavior in the low-temperature transport of quantum dots (QD's) have opened a new arena for the study of strongly correlated electrons in artificial systems. The Kondo effect in dilute magnetic alloys appears as a crossover from weak to strong coupling between delocalized electrons of the host nonmagnetic metal and the unpaired localized electron of the magnetic impurity as the temperature (T) is reduced well below the Kondo temperature (T_K).[4] This crossover leads to the formation of a singlet state between the unpaired localized electron in the impurity and electrons in the host metal. It is important, however, to emphasize the main differences of the Kondo physics in QD's with respect to bulk magnetic impurities. The parameters which define the T_K in QD's can be changed in a controlled way by applying the appropriate combination of gate voltages. So, it is possible to study either Kondo or mixed-valence regimes in the same sample. For this to be possible, there is an important requirement: the charging energy and level separation of the QD must be significantly larger than the level broadening due to the coupling to the leads. More importantly, the study of Kondo physics in QD's opens a new road to the study of *nonequilibrium* many-body phenomena, a relatively young and rich area in contemporary condensed-matter physics.

In this paper, we address the issue of a QD driven out of equilibrium by means of an ac voltage. More specifically, we study theoretically the low-temperature transport properties of a QD with an ac voltage applied to the central gate. We use a time-dependent version of the Anderson model. In its simplest formulation, the Anderson model, valid for both Kondo and mixed-valence regimes in bulk systems, describes a single discrete level with on-site electron-electron interaction coupled to a band. The model describes different physical regimes which, for QD's, are determined by the following parameters: (i) The energy difference between a discrete level in the QD (ϵ_0) and the Fermi energy of the leads (E_F). (ii) The tunneling coupling (Γ) between the discrete level in the QD and the electronic states in the reservoirs. (iii) The QD charging energy (on-site interaction U), i.e., the energy necessary to add an electron to the QD. The relevant energy scale is $T_K \simeq \sqrt{2U\Gamma}e^{-\pi[|E_F-\epsilon_0|(U+\epsilon_0)]/2\Gamma U}$, which is related to the binding energy of the many-body state.[4] For $T<T_K$, the Kondo regime is reached when $\epsilon_0 < E_F-\Gamma$ and $\epsilon_0 > E_F-U+\Gamma$ and the mixed-valence regime is established for $E_F-\Gamma<\epsilon_0<E_F$ and $E_F-U<\epsilon_0<E_F-U+\Gamma$. In the Kondo regime at $T=0$, the low-energy excitations (quasiparticles) produce a peak at E_F (Kondo resonance or Abrikosov-Suhl resonance) in the density of states (DOS).[4] One electron at E_F becomes scattered by the QD undergoing a phase shift which is proportional to the displaced charge δn [Friedel-Langreth sum rule (FLSR) (Ref. 5)] and the linear conductance for a QD symmetrically coupled to the leads takes the value $\mathcal{G}=(2e^2/h)\sin^2(\pi\delta n)$. In the symmetric case ($\epsilon_0=-U/2$), $\delta n=0.5$ leads to a perfect transparency of the QD. For any chemical potential between ϵ_0 and ϵ_0+U the QD has the linear conductance as a function of the chemical potential of an almost perfectly open channel $2e^2/h$.[6–8] This constitutes the unitary limit and has recently been experimentally verified in QD's by Van der Wiel *et al.*[9] However, as temperature increases, inelastic scattering processes reduce the DOS at E_F (i.e., the linear conductance) at the Kondo valley and eventually two peaks at ϵ_0 and ϵ_0+U appear for $T \gg T_K$.

As we already mentioned, new questions arise when driving the QD out of equilibrium.[10–23] When this is done by means of the application of a finite dc voltage bias, the linear conductance is reduced and the Kondo peak in the DOS splits.[12–14,16] More sophisticated configurations of QD's in the Kondo regime constitute a growing area of intense investigations, both from the theoretical and experimental sides. Time-dependent Kondo physics,[16] Kondo physics in integer-spin QD's,[17] QD's embedded in Aharonov-Bohm rings,[18] or double QD systems[19] are examples of such configurations.

We focus on the study of the transport properties of an Anderson Hamiltonian with a time-dependent resonant level $\tilde{\epsilon}_0(t)=\epsilon_0+V_{\rm ac}\cos(\omega_0 t)$. This can be achieved experimentally by means of a time-dependent central gate voltage capacitively coupled to the QD. In the high-temperature regime this type of experiment has indeed been carried out leading

to the observation of photon-assisted processes in the Coulomb blockade regime.[20,21] This regime has been studied theoretically as well.[22] In the same way, there has been some theoretical effort devoted to studying the ac transport at very low ($T \ll T_K$) and intermediate temperatures ($T \lesssim T_K$) in the Kondo and mixed-valence regimes.[23–29] Recently transport in an ac driven QD at low temperatures has been measured as well.[30]

In this work we clarify the role of an ac voltage in the Kondo effect in QD's. We concentrate on the low-temperature regime so that a model in the context of Fermi-liquid theory is adequate. The occupation of the QD as well as all the relevant quantities in transport have to be calculated by using nonequilibrium propagators. Finally, some approximation is needed for calculating the Green's function of the QD. Let us remark that there is not yet a nonequilibrium generalization of the theoretical tools usually employed for solving the Anderson model, i.e., Bethe ansatz,[32] numerical renormalization-group,[33] or quantum Monte Carlo methods;[34] furthermore, it is difficult to extract information about dynamical quantities from these techniques (though see Ref. 35 for a recent perturbative renormalization-group method in real time to tackle nonequilibrium situations). We choose, then, to use a finite-U perturbation theory for the Green's function of the impurity which allows us to obtain the dynamical properties at low temperatures and to generalize these quantities to a nonequilibrium situation in the whole range of interactions (U/Γ). This perturbative solution overestimates the width of the Kondo peak, i.e., T_K.[4,31] In fact, our Fermi-liquid approach gives a resonance width which decreases algebraically with U, instead of having an exponential decay as given by scaling calculations.[4] Apart from this, finite-U perturbation theory[10,36,37] gives a good description in the symmetric case, but presents clear anomalies away from this special situation (which can be overcome by means of an interpolating self-energy).[11,27] Previous efforts have concentrated on the $U \to \infty$ limit where a noncrossing approximation (NCA) (Refs. 12, 13, 23, and 26) can be made for high and intermediate temperatures. However, such approximations do not give a good description of the exact local Fermi-liquid properties as $T \to 0$. By using the NCA the transition from the weak-correlation to the strong-correlation regime is not described properly. In this paper we will restrict ourselves to the symmetric case. The study of the asymmetric case will be analyzed elsewhere.

The main difficulty for our purpose resides in the determination of the QD Green's function, and specifically the calculation of its self-energy. In a previous paper[27] we proposed an ansatz for the modification of the QD Green's function due to an harmonic modulation. Here, we improve our previous description, valid in the limit of small interaction U, and extend the calculation to finite temperatures.

The paper is organized as follows: in Sec. II we describe the theoretical model and deduce the expressions for the self-energy and the time-averaged spectral density. In Sec. III we present the results for the linear conductance and time-averaged density of states at finite temperatures and for different ac frequencies and ac intensities of the harmonic modulation. Moreover, we compare with previous theoretical models and comment on recent experimental information. Finally, Sec. IV summarizes the main conclusions of the paper.

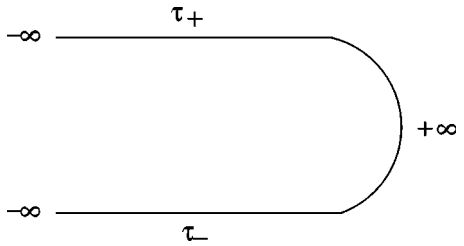

FIG. 1. Complex time contour. The times in the positive branch are τ_+ while times in the negative branch are τ_-.

II. THEORETICAL MODEL

A. Keldysh formalism

The application of a time-dependent component to the energy level in the Anderson Hamiltonian [see Eq. (3) below] breaks the time translational invariance of the system and, then, we need an approach capable of addressing this fully nonequilibrium situation. When the time-dependent perturbation acts for a while, the system does not recover its thermodynamic equilibrium after the perturbation is over. The whole process does not have the symmetry between $t \to -\infty$ and $t \to \infty$ and, then, an equilibrium expansion in terms of expectation values is not possible. Nevertheless, the problem can be solved by allowing the system to evolve from $-\infty$ to the moment of interest $\bar{t}$ and then continuously evolve from $t=\bar{t}$ back to $t \to -\infty$. In this way all the expectation values are evaluated in a well-defined state which was prepared in a remote past. This special complex time contour (see Fig. 1) is the main ingredient of the nonequilibrium Keldysh formalism.[38] In the conventional Keldysh matrix formulation of the perturbation theory, one does not work directly with the Green's function defined on the complex time contour, but with a linear combination of the four possible time orders. The usual linear combinations are (similar relations hold for the self-energies)

$$G^r_{d,\sigma}(t,t') = \theta(t-t')[G^>_{d,\sigma}(t,t') - G^<_{d,\sigma}(t,t')],$$

$$G^a_{d,\sigma}(t,t') = \theta(t'-t)[G^<_{d,\sigma}(t,t') - G^>_{d,\sigma}(t,t')], \qquad (1)$$

where $G^r_{d,\sigma}(t,t')$ is the retarded Green's function, $G^a_{d,\sigma}(t,t')$ is the advanced Green's function, and $G^<_{d,\sigma}(t,t')$, $G^>_{d,\sigma}(t,t')$ are the so-called lesser and greater Green's functions, respectively.

B. Hamiltonian

The time-dependent Anderson Hamiltonian is:

$$H = H_{\text{leads}} + H_{\text{QD}} + H_{\text{sd}} + H_{\text{ac}}(t), \qquad (2)$$

where

$$H_{\text{leads}}=\sum_{k\in\{L,R\},\sigma}\epsilon_k c^{\dagger}_{k,\sigma},c_{k,\sigma},$$

$$H_{QD}=\sum_{\sigma}\epsilon_{0,\sigma}d^{\dagger}_{\sigma}d_{\sigma}+Ud^{\dagger}_{\uparrow}d_{\uparrow}d^{\dagger}_{\downarrow}d_{\downarrow},$$

$$H_{sd}=\sum_{k\in\{L,R\},\sigma}V_k c^{\dagger}_{k,\sigma}d_{\sigma}+V^{*}_{k}d^{\dagger}_{\sigma}c_{k,\sigma},$$

$$H_{\text{ac}}(t)=\sum_{\sigma}V_{\text{ac}}\cos\omega_0 t\, d^{\dagger}_{\sigma}d_{\sigma}. \tag{3}$$

V_{ac} and ω_0 are the ac intensity and ac frequency of the ac potential respectively. $d^{\dagger}_{\sigma}$ creates an electron with spin σ in the QD, while $c^{\dagger}_{k,\sigma}$ creates it in the lead with energy ϵ_k (k labels the rest of quantum numbers). The ac voltage modulates in time the relative position of the QD level $\epsilon_{0,\sigma}$ with respect to E_F. An eventual breakdown of the spin degeneracy would be represented by $\epsilon_{0,\sigma}\neq\epsilon_{0,\bar{\sigma}}$. The coupling V_k between the QD and the leads produces a broadening

$$\Gamma^{L(R)}(\epsilon)=-2\,\text{Im}[\Sigma^{L(R)}_{sd}(\epsilon+i\delta)]$$
$$=2\pi\Sigma_{k\in L(R)}|V_k|^2\delta(\epsilon-\epsilon_k),$$

where $\Sigma^{L(R)}_{sd}$ is the hybridization single-particle retarded self-energy. Hereafter, for simplicity, we consider the wide band (WB) limit approximation which neglects the principal value of the hybridization self-energy and considers the imaginary part to be an energy-independent constant, i.e., $\Sigma^{L(R)}_{sd}(\epsilon)=\Lambda^{L(R)}(\epsilon)-i\Gamma^{L(R)}(\epsilon)/2\approx-i\Gamma^{L(R)}/2$.

C. Model

Here, we discuss the procedure for obtaining the QD Green's functions which allows us to obtain the spectral density of the QD and the linear conductance. In the remote past, the QD is decoupled from the leads. The coupling between different regions (the contacts and the central region) is treated as a perturbation by means of standard equilibrium perturbation theory. In a first step, the effect of the on-site interaction is included via a Hartree mean-field approximation (see Appendix A). The time modulation of the QD level is treated via nonequilibrium perturbation theory, since the time translational invariance is broken by the ac voltage. At this point, we include the correlation effects by computing the on-site interaction self-energy (lesser and greater) up to second order by means of the diagrams of Fig. 2. These diagrams are evaluated by using the previous lesser and greater Green's functions as bare propagators (Appendix B). These bare propagators include the coupling between the QD and the contacts, the time dependence of the QD level, and the on-site interaction in the Hartree approximation. Once the correlation self-energy has been calculated, the QD retarded Green's function is obtained by means of the time-dependent Dyson equation [Eq. (10)]. Finally, the time-averaged spectral density [Eq. (18)] and the linear conductance [Eq. (19)] are calculated from the QD retarded Green's function.

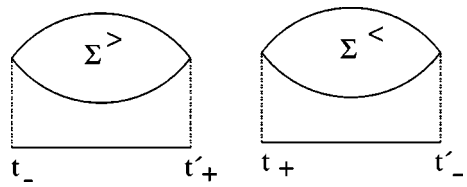

FIG. 2. Self-energies of order U^2, $\Sigma^{>,(2)}_{d,\sigma}(t,t')$, and $\Sigma^{<,(2)}_{d,\sigma}\times(t,t')$. The times in the causal branch are marked with a + symbol whereas the times in the anticausal branch are marked with a − symbol. Solid lines denote QD Green's functions in the Hartree approximation including coupling to the leads and ac potential. Dashed lines correspond to the on-site repulsion U electron-electron interaction.

D. Correlation self-energy

The starting point for the derivation of the correlation self-energy in the presence of the ac potential consists of calculating the lesser and greater QD Green's functions, in the Hartree approximation, including coupling to the leads. In the absence of the time-dependent potential, the retarded and advanced QD Green's functions have the following expressions (see Appendix A):

$$\mathbf{g}^{r,a}_{d,\sigma}(t-t')=\mp i\,\theta(\pm t\mp t')$$
$$\times\exp^{-i\int_{t'}^{t}dt_1(\epsilon_{0,\sigma}+Un_{d,\bar{\sigma}}\mp i\Sigma_{\alpha\in L,R}\Gamma_{\alpha}/2)}, \tag{4}$$

$n_{d,\sigma}=\langle d^{\dagger}_{\sigma}(t)d_{\sigma}(t)\rangle$ being the QD occupation. Note that these QD Green's functions have been calculated taking into account the coupling self-energy (which is given by $\mp i\Sigma_{\alpha\in L,R}\Gamma_{\alpha}/2$) and the interaction in the Hartree approximation (given by $Un_{d,\bar{\sigma}}$). Now, if one also considers a time modulation of the QD level, the retarded and advanced QD Green's functions have the following forms (see Appendix B)

$$G^{r,a}_{d,\sigma}(t,t')=e^{-i(V_{\text{ac}}/\omega_0)(\sin\omega_0 t-\sin\omega_0 t')}\mathbf{g}^{r,a}_{d,\sigma}(t-t'). \tag{5}$$

The lesser and greater QD Green's functions can be obtained through the well-known relation[39,41]

$$G^{<,>}_{d,\sigma}(t,t')$$
$$=\int dt_1\int dt_2 G^{r}_{d,\sigma}(t,t_1)\Sigma^{<,>}_{sd}(t_1,t_2)G^{a}_{d,\sigma}(t_2,t'), \tag{6}$$

where $\Sigma^{<,>}_{sd}(t_1,t_2)$ are the lesser and greater coupling self-energies defined in Appendix A [Eqs. (A2) and (A3), respectively]. Now we include correlation effects up to second order in the on-site Coulomb interaction (see Fig. 2). The new lesser and greater correlation self-energies are calculated by means of the diagrams of Fig. 2 with bare lines which are given by the propagators of Eq. (6) [analytical expressions are given in Appendix B, Eqs. (B8)–(B11)]:

$$\Sigma^{>,(2)}_{d,\sigma}(t,t')=iU^2G^{>}_{d,\sigma}(t,t')G^{<}_{d,\bar{\sigma}}(t',t)G^{>}_{d,\bar{\sigma}}(t,t'), \tag{7}$$

and

$$\Sigma^{<,(2)}_{d,\sigma}(t,t')=-iU^2G^{<}_{d,\sigma}(t,t')G^{>}_{d,\bar{\sigma}}(t',t)G^{<}_{d,\bar{\sigma}}(t,t'). \quad (8)$$

The retarded self-energy

$$\Sigma^{r,(2)}_{d,\sigma}(t,t')=\theta(t-t')[\Sigma^{<,(2)}_{d,\sigma}(t,t')-\Sigma^{>,(2)}_{d,\sigma}(t,t')] \quad (9)$$

is obtained from Eqs. (7) and (8).

E. Dyson equation

The next step for deriving the retarded QD Green's function consists of solving the retarded time-dependent Dyson equation. By using Eq. (9) for the self-energy, one can write

$$\left[i\frac{\partial}{\partial t}-\left(\bar{\epsilon}_{0,\sigma}(t)-i\sum_{\alpha\in L,R}\Gamma_\alpha/2\right)\right]\mathbf{G}^{r,(2)}_{d,\sigma}(t,t') = \delta(t-t')+\int dt_1\Sigma^{r,(2)}_{d,\sigma}(t,t_1)\mathbf{G}^{r,(2)}_{d,\sigma}(t_1,t'), \quad (10)$$

where $\bar{\epsilon}_{0,\sigma}(t)=\epsilon_{0,\sigma}+Un_{d,\bar{\sigma}}(t)+V_{\rm ac}\cos\omega_0 t$. In the symmetric case $n_{d,\sigma}=n_{d,\bar{\sigma}}=1/2$, which allows us to close the Dyson equation for the retarded Green's function [Eq. (10)] without any further self-consistency in the lesser part. Equation (10) simplifies considerably by making the gauge transformation

$$\mathbf{G}^{r,(2)}_{d,\sigma}(t,t')=-i\theta(t-t')e^{-i\int_{t'}^{t}d\tau[\bar{\epsilon}_{0,\sigma}(\tau)-i\sum_{\alpha\in L,R}\Gamma_\alpha/2]}\bar{\mathbf{g}}_\sigma(t,t'). \quad (11)$$

In the presence of time modulation, the retarded Dyson equation becomes

$$\frac{\partial}{\partial\bar{t}}\bar{\mathbf{g}}_\sigma(t,t')=-\int_{t'}^{t}dt_1K_\sigma(t,t_1)\bar{\mathbf{g}}_\sigma(t_1,t'), \quad (12)$$

which is defined only for $t\geqslant t'$ due to the θ function appearing in Eq. (11). $K_\sigma(t,t')$ is the kernel of the integrodifferential time-dependent Dyson equation which is related to the retarded self-energy through the relation

$$\Sigma^{r,(2)}_{d,\sigma}(t,t_1)=-i\theta(t-t_1)K_\sigma(t,t_1) \times e^{-i\int_{t_1}^{t}d\tau[\bar{\epsilon}_{0,\sigma}(\tau)-i\Sigma_{\alpha\in L,R}\Gamma_\alpha/2]}. \quad (13)$$

When $t=t'$, an additional condition must be imposed in Eq. (10): $\mathbf{G}^{r,(2)}_{d,\sigma}(t,t)=-i\langle\{d_\sigma(t),d^\dagger_\sigma(t)\}\rangle=-i$, where $\{\}$ is the anticommutator. This condition implies that the solution of Eq. (12) when $t=t'$ is $\bar{\mathbf{g}}_\sigma(t,t)=1$.

We solve Eq. (12) by discretizing the temporal variables, the partial derivative is replaced by the finite difference

$$\frac{\partial}{\partial\bar{t}}\bar{\mathbf{g}}_\sigma(t,t')\rightarrow\frac{\bar{\mathbf{g}}_\sigma(m,n)-\bar{\mathbf{g}}_\sigma(m-1,n)}{\delta}, \quad (14)$$

where δ is the grid spacing in time space. The integral is converted into a sum

$$\int_{t'}^{t}dt_1K_\sigma(t,t_1)\bar{\mathbf{g}}_\sigma(t_1,t')\rightarrow\delta\sum_{k=n}^{m}c_kK_\sigma(m,k)\bar{\mathbf{g}}_\sigma(k,n). \quad (15)$$

Now, the indexes m, n, and k replace the time arguments which appear in Eq. (12). The coefficients c_k are equal to 1 except when $m=k$ or $n=k$ in which $c_k=\frac{1}{2}$. In this way, the discretized time-dependent Dyson equation has the following form:

$$\bar{\mathbf{g}}_\sigma(m,n)=\bar{\mathbf{g}}_\sigma(m-1,n)-\delta^2\sum_{k=n}^{m}c_kK_\sigma(m,k)\bar{\mathbf{g}}_\sigma(k,n). \quad (16)$$

Equation (16) constitutes a set of linear equations that can be solved by standard numerical techniques. Its solution gives the retarded QD Green's function which is used to study the transport properties of the system in the next section.

F. Time-averaged spectral density and linear conductance

The time-dependent spectral density $\rho_\sigma(\epsilon,\bar{t})$, being $\bar{t}=(t+t')/2$, is defined as the imaginary part of the Fourier transform with respect to $\tau=t-t'$ of the retarded QD Green's function,

$$\rho_\sigma(\epsilon,\bar{t})=-\frac{1}{\pi}\mathrm{Im}\int_{-\infty}^{\infty}\mathbf{G}^{r,(2)}_{d,\sigma}(\bar{t}+\tau/2,\bar{t}-\tau/2)e^{i\epsilon\tau}d\tau. \quad (17)$$

Since the measurement of the linear conductance implies a time-average in $\bar{t}$, we work with the time-averaged spectral density which reads

$$\langle A_\sigma(\epsilon)\rangle=\frac{\omega_0}{2\pi}\int_0^{2\pi/\omega_0}d\bar{t}\rho_\sigma(\epsilon,\bar{t}). \quad (18)$$

The linear conductance[39] at finite temperature, in terms of the time-averaged spectral density, is given by

$$\mathcal{G}=\frac{e^2}{\hbar}\int d\epsilon\frac{\Gamma_L\Gamma_R}{\Gamma_L+\Gamma_R}\left(-\frac{\partial f(\epsilon)}{\partial\epsilon}\right)\sum_\sigma\langle A_\sigma(\epsilon)\rangle, \quad (19)$$

where $f(\epsilon)$ is the Fermi-Dirac distribution function.

III. RESULTS

We solve numerically the set of linear Eqs. (16) for a QD in the Kondo regime (symmetric case $\epsilon_0=-U/2$ with symmetric couplings $\Gamma_L=\Gamma_R=\Gamma$ and $U=2.5\pi\Gamma$) at finite temperature $T=0.05\Gamma$ for different ac frequencies and ac intensities. As we already mentioned, our perturbation scheme in the on-site interaction overestimates T_K. Nevertheless, it is possible to extract an energy scale characterizing spin fluctuations T_K from the half-width of the many body Kondo resonance at E_F.[4] Also worth mentioning is the fact that, according to this definition, T_K acquires a clear physical meaning in our Fermi-liquid context: at a finite temperature $T\sim T_K$ the unitary limit for scattering has been reduced to 1/2.[4] In our case, symmetric configuration with $U=2.5\pi\Gamma$, the corresponding Kondo temperature is $T_K\approx0.24\Gamma$, i.e., $T\ll T_K$. The Fermi-liquid theory is, then, a good approximation to describe the dynamical and transport properties of the QD. We obtain, from the solution of Eq. (16) for the retarded Green's function, the time-averaged density of states [Eq. (18)] and the linear conductance [Eq. (19)].

The main effect of the ac potential consists in a reduction of the time-averaged DOS at E_F. This reduction can be interpreted as decoherence induced by ac excitations, either by real photon-assisted induced excitations at large ac frequencies[26] or virtual spin-flip cotunneling processes at small ac frequencies.[29] These processes introduce a quenching of the Kondo peak causing a deviation of the linear conductance from the unitary limit. It is difficult to extract the magnitude of this lifetime induced by the ac from our analytical expressions for the self-energies. Instead, in the next paragraphs, we present a simple estimate for the lifetime via a perturbative argument and try to relate this simple perturbative result with our full calculation.

A. Rate of spin-flip cotunneling processes

In the case of spin-flip cotunneling the simplest process involves the hopping of one electron out of the dot to a state above the Fermi level while another electron in the reservoirs, with opposite spin, enters into the dot. The rate of virtual spin-flip cotunneling which takes into account one photon processes is restricted to the case of very low ac frequencies and amplitudes, i.e, $\omega_0, V_{\rm ac} \ll \epsilon_0, \epsilon_0+U$. Under these conditions the rate of spin-flip cotunneling was derived in Ref. 29. In the symmetric case the rate obtained there is zero. Without restrictions, the expression for the rate can be generalized quite easily. By means of a modified Schrieffer-Wolff transformation[28,29] accounting for the time dependence of the parameters of the Hamiltonian (3) one can describe the QD system in terms of a Kondo Hamiltonian with a time-dependent coupling constant,

$$J_{\alpha,\alpha'}(t)=\frac{\sqrt{\Gamma_\alpha\Gamma_{\alpha'}}}{4\pi\rho_{\rm leads}}\sum_{n,m}J_n(\beta)J_m(\beta)e^{i[(n-m)\omega_0 t]}\left(\frac{1}{\epsilon_0+n\omega_0}-\frac{1}{\epsilon_0+U+n\omega_0}+\frac{1}{\epsilon_0+m\omega_0}-\frac{1}{\epsilon_0+U+m\omega_0}\right), \tag{20}$$

where $\mathbf{J}n(\beta)$ is the Bessel function of order n and argument $\beta=V_{\rm ac}/\omega_0$. To second order in the time-dependent coupling constant [Eq. (20)] the rate of spin-flip cotunneling can be found as

$$\gamma=\frac{1}{2\pi}\sum_{\alpha\alpha',n,m}(\mathbf{J}^{n,m}_{\alpha\alpha'})^2|n-m|\omega_0, \tag{21}$$

where $\mathbf{J}_{\alpha\alpha'}$ is

$$\mathbf{J}^{n,m}_{\alpha\alpha'}=\frac{\sqrt{\Gamma_\alpha\Gamma_{\alpha'}}J_n(\beta)J_m(\beta)}{4}\left(\frac{1}{\epsilon_0+n\omega_0}-\frac{1}{\epsilon_0+U+n\omega_0}+\frac{1}{\epsilon_0+m\omega_0}-\frac{1}{\epsilon_0+U+m\omega_0}\right). \tag{22}$$

In the limit of very low ac frequencies and taking into account one-photon processes, we recover from Eq. (21) the expression derived in Ref. 29 [Eq. (41)]: $\gamma=(\omega_0/8\pi)[(\Gamma_L+\Gamma_R)U/(U+\epsilon_0)]^2[V_{\rm ac}(U+2\epsilon_0)/(\epsilon_0+U)\epsilon_0]^2$. Equation (21) shows that the rate of spin-flip cotunneling depends on the absorption or emission probability of photons through the Bessel functions, the energy denominators, and the window of energy given by $|n-m|\omega_0$, its behavior as a function of the ac frequency depends on two opposite effects. On one hand, by increasing ω_0 the window of allowed states becomes larger but on the other hand the absorption or emission probability diminishes. The competition of these two opposite effects produces a maximal rate at certain frequency ω_c.

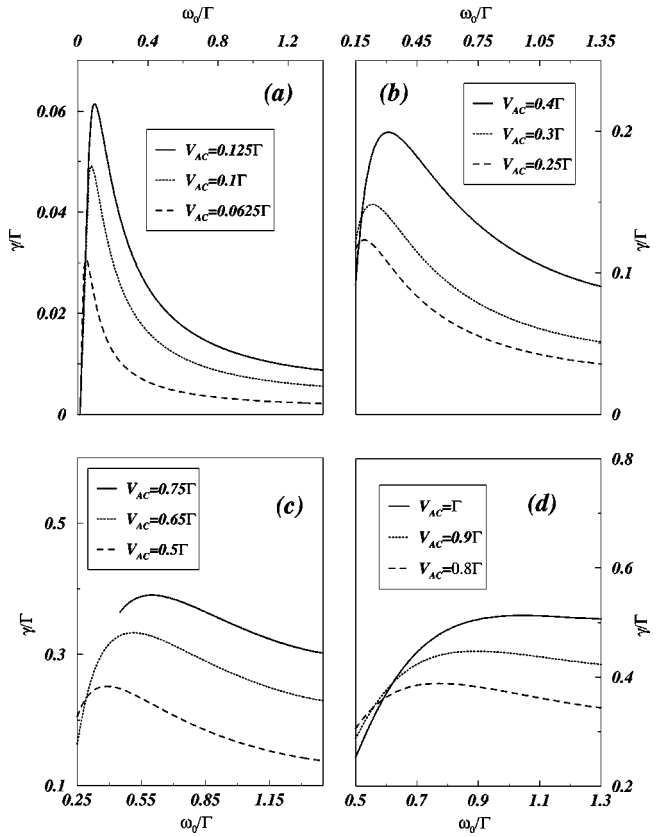

FIG. 3. Spin-flip cotunneling rate as a function of ω_0 for various ac amplitudes. (a) shows the case of very low ac amplitudes, for $\omega_0<\omega_c$ the rate grows linearly. (b) depicts the rate for different ac amplitudes in a range of ac frequencies from $\omega_0=0.15\Gamma\approx T_K/2$ to $\omega_0=\Gamma\approx 4T_K$. (c) and (d) exhibit the case of intense irradiation where the Kondo peak is strongly quenched.

In Fig. 3 the decoherence rate [Eq. (21)] is plotted as a function of the ac frequency for different ac intensities. For low ac intensities and low ac frequencies the rate grows linearly with ω_0 as expected. ω_c moves to higher values as the ac amplitude increases. The behavior of ω_c as a function of $V_{\rm ac}$ is linear (Fig. 4). We can conclude from the slope of this curve that $\omega_c/V_{\rm ac}\approx 0.9$ (or $\beta\approx 1.1$).

These results can be connected with our numerical calculations for the conductance, see below, by using the exact Anderson model relation for the scattering rate.[4,26] This quantity gives the total rate at which lead electrons of energy E_F suffer intralead and interlead scattering by the QD,

$$\pi\Delta=\pi\sum_{KEL,R}|V_k|^2\langle A(E_F)\rangle=\frac{\pi}{2}\frac{(\Gamma_L+\Gamma_R)}{\rho_{\rm leads}}\langle A(E_F)\rangle, \tag{23}$$

where $\langle A(E_F)\rangle$ [Eq. (18)] is the time-averaged spectral function at the Fermi level. In the absence of irradiation and for

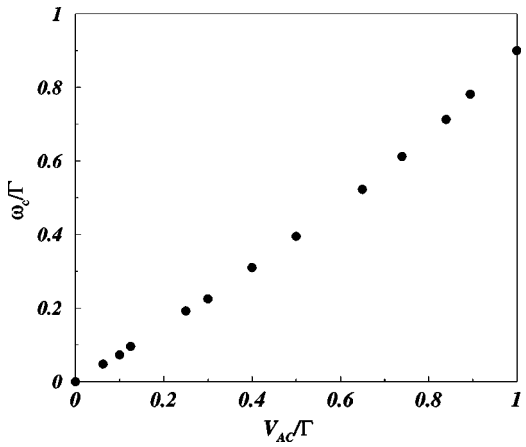

FIG. 4. ω_c as a function of the ac intensity.

symmetric couplings the scattering rate can be obtained by using the FLSR in the symmetric case as

$$\pi\Delta\rho_{\text{leads}}=\frac{\Gamma^2}{[\Gamma-\text{Im}\,\Sigma^r_{\text{int}}(E_F)]^2}, \tag{24}$$

where $\Sigma^r_{\text{int}}(E_F)$ is the proper interaction self-energy at the Fermi level. At $T=0$ the scattering rate reaches the unitary limit ($\pi\rho_{\text{leads}}\Delta=1$) since the low-energy excitations have an infinite lifetime, i.e., $\text{Im}\,\Sigma_{\text{int}}(E_F)=0$. A finite lifetime induced by any decoherence source reduces the scattering rate. Intuitively, one can argue that the main role of the ac potential is to induce decoherence in the Kondo state by introducing a finite lifetime (even at $T=0$). We can define an effective time-averaged self-energy $\langle\Sigma^{\text{ac}}_{\text{int}}(E_F)\rangle$ in the presence of irradiation such that the time-averaged DOS at E_F can be written as

$$\pi\Gamma\langle A(E_F)\rangle=\frac{\Gamma^2}{[\Gamma-\text{Im}\langle\Sigma^{\text{ac}}_{\text{int}}(E_F)\rangle]^2}. \tag{25}$$

With this notation, one can identify the imaginary part of this effective self-energy as the total rate of decoherence induced by the ac potential, including the spin-flip cotunneling derived above, i.e., $\nu=-\text{Im}\langle\Sigma^{\text{ac}}_{\text{int}}(E_F)\rangle$. We plot in Fig. 5(a) the rate of spin-flip cotunneling and the total decoherence rate obtained from our calculations versus ω_0. Both rates present a maximum. It is obvious, then, from the behavior of the total decoherence rate versus ω_0, that the linear conductance presents a minimum at a critical frequency.

From the dependence of the decoherence rate on the ac parameters and from the energy scale for spin fluctuations T_K we can define two different regimes for the ac Kondo problem: (i) *Weak reduction* regime occurs when $\nu/T_K<1$. In this case, the formation time for the Kondo state [given by $1/T_K$ (Ref. 40)] is shorter than the necessary time to destroy it, which is given by the inverse of the decoherence rate, and the system spends most of the time in a Kondo state without or with little decoherence. On average, this translates into a high linear conductance independently of the applied ac parameters. As long as the photon absorption or emission rate is negligible, and therefore the ac is not effective for inducing decoherence, it is irrelevant whether or not the frequency is larger or smaller than T_K (see Fig. 3). (ii) *Strong reduction* regime is found when $\nu/T_K>1$. In this case, the decoherence time is shorter than $1/T_K$ and the system spends most of the time in a state with a strong reduction of the Kondo effect.

B. Conductance as a function of the ac parameters

To illustrate the previous discussion we plot the conductance as a function of ω_0, at a fixed ac intensity [in Fig. 6(a) for $V_{\text{ac}}<\Gamma$ and in Fig. 7(a) for $V_{\text{ac}}\geqslant\Gamma$]. In both cases we find that there are two different behaviors separated by a critical frequency ω_c, where the conductance presents a minimum. As we already mentioned, the presence of this minimum is regulated by the competition of two opposite effects. In the adiabatic limit, where $\omega_0\to 0$, the effect of the applied ac potential has a negligible effect on the dynamics of the correlated collective state (*weak reduction* regime). In

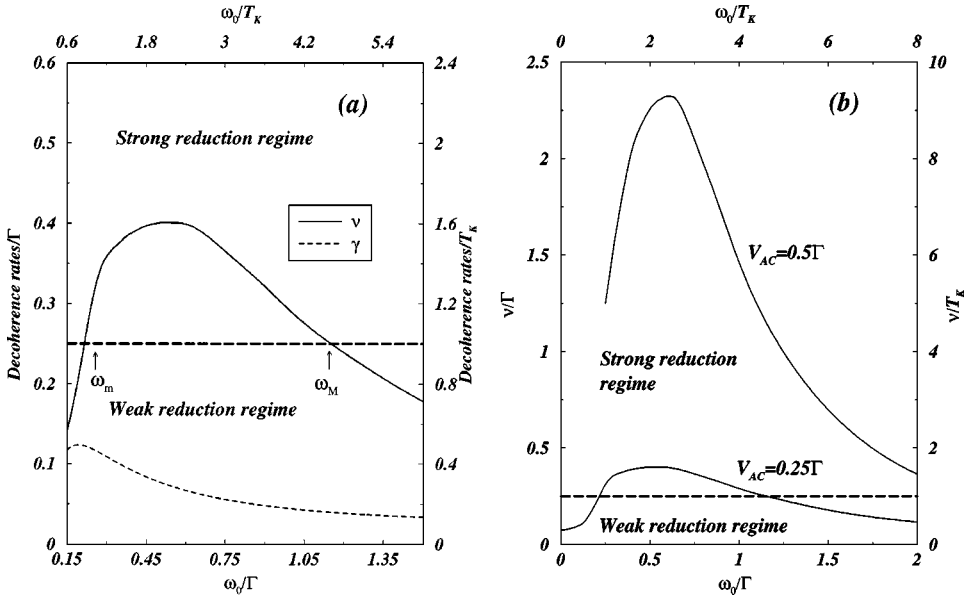

FIG. 5. (a) Rate of decoherence vs ω_0 for $V_{\text{ac}}=0.25\Gamma\approx 2T_K$. The solid line shows the total rate of decoherence obtained from the numerical results, the dotted line depicts the rate of spin-flip cotunneling derived from Eq. (21) as a function of ω_0. (b) Total rate of decoherence vs ω_0 for two intensities: $V_{\text{ac}}=0.25\Gamma\approx T_K$ and $V_{\text{ac}}=0.5\Gamma\approx 2T_K$. Strong and weak reduction regimes are separated by the horizontal line $\nu=T_K$. For $\omega_0<\omega_m$ and $\omega_0>\omega_M$ the system is found in the weak reduction regime and the strong reduction regime is achieved for $\omega_m<\omega_0<\omega_M$.

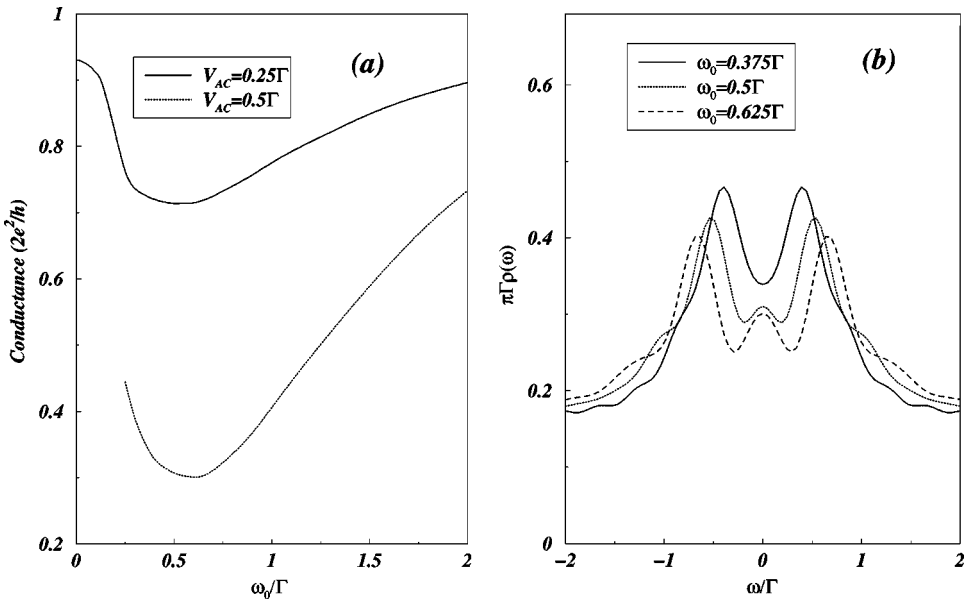

FIG. 6. (a) Conductance as a function of ω_0. The solid line shows the case of $V_{\rm ac}=0.25\Gamma \approx T_K$, the dotted line corresponds to the case of stronger ac intensity $V_{\rm ac}=0.5\Gamma \approx 2T_K$. (b) Time-averaged DOS for the cases of $\omega_0=0.375\Gamma \approx 3T_K/2$ (solid line), $\omega_0=\Gamma/2 \approx 2T_K$ (dotted line), $\omega_0=0.625\Gamma \approx 5T_K/2$ (dashed line) for a fixed AC amplitude $V_{\rm ac}=0.5\Gamma \approx 2T_K$.

this case, the quenching of the Kondo peak is no longer effective and therefore the ac only induces a small decoherence in the singlet state. In the very high ac frequency limit, where $\omega_0 \to \infty$ (in this limit $\beta \to 0$), the unpaired electron has a negligible absorption probability and one reaches again the *weak reduction* regime, i.e., $\nu/T_K < 1$. For the lowest ac amplitude in Fig. 6(a) (solid line, $V_{\rm ac}=0.25\Gamma$) the QD is in the *weak reduction* regime for ac frequencies below $\omega_m \sim 0.2\Gamma$ and frequencies above $\omega_M \sim 1.2\Gamma$ [see Fig. 5(b)]. The *strong reduction* regime ($\nu/T_K > 1$) is reached for frequencies $\omega_m < \omega_0 < \omega_M$. By doubling the ac amplitude [$V_{\rm ac}=0.5\Gamma$, dotted line in Fig. 6(a)] the QD enters in the *strong reduction* regime for all the frequencies studied [from Fig. 5(b), the rate is above the line $\nu/T_K=1$ for all the frequencies]. The critical frequency depends on the ac amplitude: for $V_{\rm ac}=0.25\Gamma$ $\omega_c \approx 0.5\Gamma$ and for $V_{\rm ac}=0.5\Gamma$ $\omega_c \approx 0.625\Gamma$. For $\omega_0 < \omega_c$ the behavior of the conductance qualitatively follows that of the spin-flip rate shown in Fig. 3(b): the slowest drop of conductance corresponds to the smallest ac amplitude. This competition of opposite effects giving a minimum in conductance vs ω_0 is illustrated in Fig. 6(b), where we plot the time-averaged DOS at E_F for three ac frequencies $\omega_0 \leqslant \omega_c$. By increasing the ac frequency from $\omega_0=0.375\Gamma$ up to $\omega_0=0.5\Gamma$ the Kondo resonance is suppressed more effectively than by raising the ac frequency from $\omega_0=0.5\Gamma$ up to $\omega_0=0.625\Gamma$ where the reduction of the Kondo peak is almost negligible. Figure 7(a) depicts the conductance vs ω_0 for $V_{\rm ac} \geqslant \Gamma$. Remarkably, we find $\omega_c/V_{\rm ac} \simeq 1$ in a good agreement with the tendency found in Fig. 4. Here again the suppression of the conductance is smaller for the lowest ac amplitude. Furthermore, in the region where the conductance is an increasing function of the ac frequency, this increase is slower for the highest ac intensity. The previous behavior is illustrated in Fig. 7(b) where we plot the time-averaged DOS

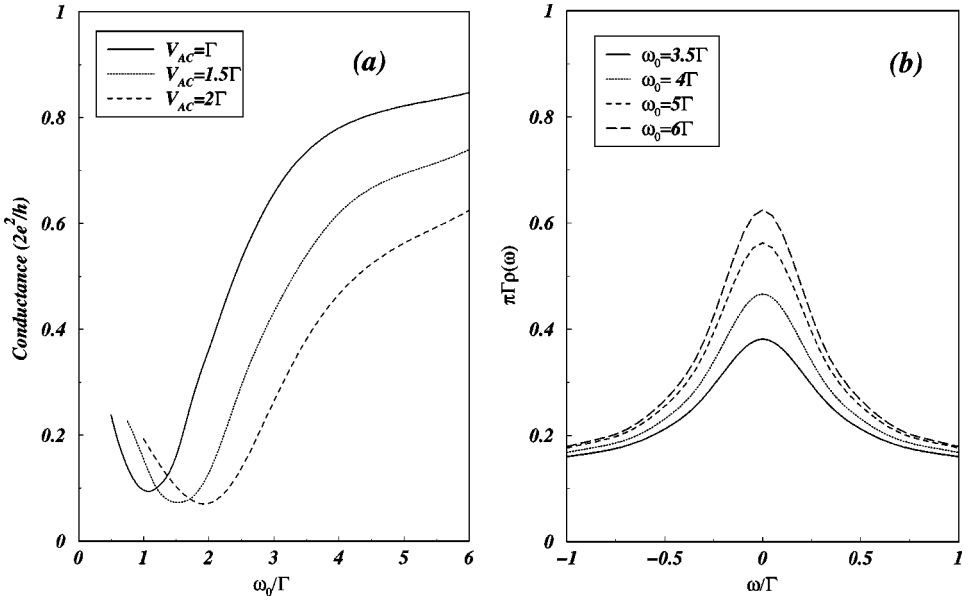

FIG. 7. (a) Conductance as a function of ω_0 and different intensities: $V_{\rm ac}=\Gamma \approx 4T_K$ (solid line), $V_{\rm ac}=1.5\Gamma \approx 6T_K$ (dotted line), $V_{\rm ac}=2\Gamma \approx 8T_K$ (dashed line). (b) Time-averaged DOS for $V_{\rm ac}=2\Gamma$ and different ac frequencies: solid line $\omega_0=3.5\Gamma \approx 14T_K$ ($\beta=0.57$), dotted line $\omega_0=4\Gamma \approx 16T_K$ ($\beta=0.5$), dashed line $\omega_0=5\Gamma \approx 20T_K$ ($\beta=0.22$), and long-dashed line $\omega_0=6\Gamma \approx 24T_K$ ($\beta=0.16$).

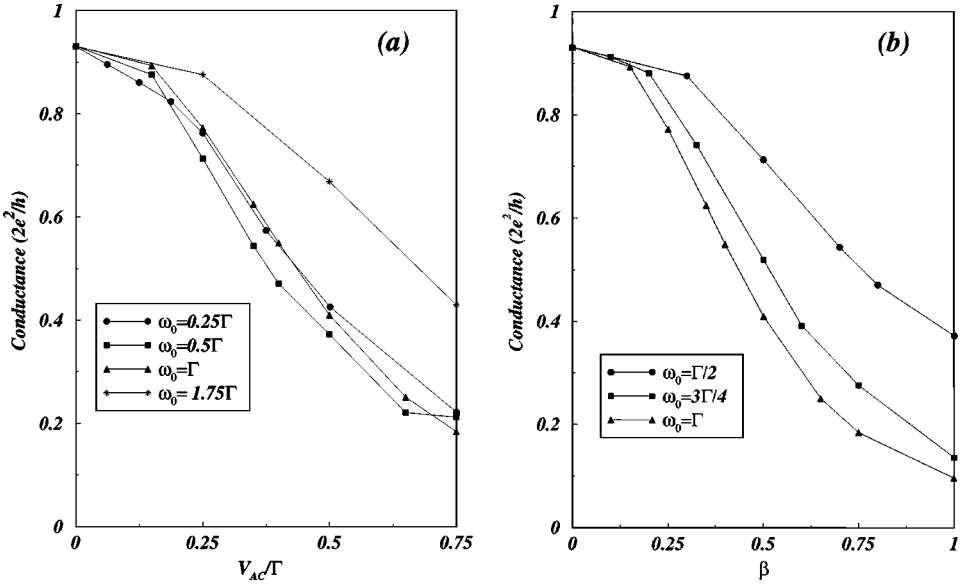

FIG. 8. (a) Conductance as a function of $V_{\rm ac}$ for four ac frequencies. (b) Conductance vs β for three ac frequencies.

for several ac frequencies at the strongest ac intensity $V_{\rm ac}=2\Gamma$. In this regime the Kondo peak always increases as ω_0 does.

Let us now compare our results with the ones obtained with different schemes:[29,26] Kaminski *et al.*[29] predict no suppression of the Kondo peak for the symmetric case ($\epsilon_0=-U/2$) in clear disagreement with both our theory and experimental results.[30] Their analysis of the ac Kondo problem is based on a decoherence rate obtained for the case where one takes into account one photon processes at very low ac frequencies. In asymmetric cases, they predict a monotonous decrease of the height of the Kondo peak as a function of ω_0. Their results (for $\epsilon_0\neq -U/2$) show that increasing the ac frequency the Kondo peak declines. Our results (for $\epsilon_0=-U/2$) show, as well, a decay of the Kondo peak in the low ac frequency regime as ω_0 grows [see Fig. 6(a)]. The rest of the cases discussed here are away from the range of validity of Ref. 29. Our study of the ac Kondo problem has been restricted to the symmetric case which is relevant in the experiment. However, we expect a similar behavior in the Kondo regime away from the symmetric configuration [the rate of the spin-flip cotunneling presents the same behavior as a function of the ac parameters for asymmetric cases; see Eq. (21)].

Using a NCA, Nordlander *et al.*[26] found a nonmonotonous behavior of the conductance vs ω_0 and the existence of a minimum, in qualitative agreement with us. In addition Nordlander *et al.* found oscillations in the conductance as a function of the ac frequency for asymmetric configurations. These oscillations come from charge fluctuations induced by the ac potential when ω_0 approximately equals the ionization energy ϵ_0. In our particle-hole symmetric configuration charge fluctuations are not possible and, then, our results do not show such oscillations. Thus caution is needed in comparing both works due to the different approximations involved and the different regimes of validity for both calculations. Whereas our perturbative calculation is valid for the symmetric case, and low temperatures, the NCA considers the limit $U\rightarrow\infty$ (i.e., the strongly asymmetric case) and temperatures of the order and higher than T_K. In that sense, both calculations should be regarded as complementary. The dependence of the conductance as a function of the ac amplitude is shown in Fig. 8(a) for four different ac frequencies. The height of the Kondo peak falls off as the applied ac intensity increases. Again, we can explain our results in simpler terms by relating them to the rate of spin-flip cotunneling [Eq. (21)]. Figure 8(b) plots the conductance as a function of β for three different ac frequencies. From this figure one can conclude that for the same value of β (same absorption probability of photons) the maximal reduction in the conductance is reached for the largest ac frequency as one should expect.

Experimentally there was found an almost universal behavior of the conductance as a function of β.[30] It is important to note, however, that in the experiment the ac amplitude of the radiation seen by the electrons in the QD depends on the attenuation which is ac frequency dependent. In our calculation, attenuation effects, which depends on complicated circuit-dependent parameters, are not included and, then, a direct comparison with the experimental results is beyond the scope of our work. Let us mention only that the experimental scales for spin and charge fluctuations are very close, $T_K\sim\Gamma/2\sim 100\ \mu$eV$\sim 25$ GHz. It is difficult, then, to separate contributions coming from spin-flip related Kondo physics to those coming from charge fluctuations.

C. Time-averaged density of states

Another important question in the ac Kondo problem is if the sidebands of the Kondo peak induced by the irradiation can be observed. In order to investigate when the Kondo state develops sidebands we plot in Fig. 9 the time-averaged DOS for three different ac frequencies, $\omega_0=\Gamma/4\approx T_K$ [Fig. 9(a)], $\omega_0=\Gamma/2\approx 2T_K$ [Fig. 9(b)] and $\omega_0=\Gamma\approx 4T_K$ [Fig. 9(c)]. For each ac frequency we consider different ac intensities corresponding to $\beta=0$, 0.25, 0.5, and 0.75. We have chosen the β parameter since this one regulates the absorption or emission probability of photons. Figure 9(a) corre-

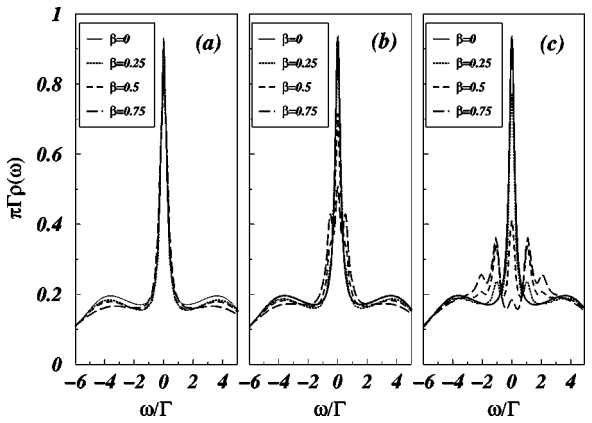

FIG. 9. Time-averaged DOS. (a) The ac frequency is $\omega_0=\Gamma/4 \approx T_K$, the solid line is the case in the absence of the ac potential, i.e., $\beta=0$, where $\beta=V_{\rm ac}/\omega_0$. In this case the peak at E_F reaches a height of 0.93. The dotted line corresponds to $\beta=0.25$ ($V_{\rm ac}=0.0625\Gamma\approx T_K/4$). The dashed line shows the case of $\beta=0.5$ ($V_{\rm ac}=0.125\Gamma\approx T_K/2$). The dot-dashed line corresponds to $\beta=0.75$ ($V_{\rm ac}=0.1875\Gamma\approx 3T_K/4$). In the three cases the Kondo peak is slightly reduced by the ac signal. (b) $\omega_0=\Gamma/2\approx 2T_K$. The solid line corresponds to $\beta=0$, the dotted line to $\beta=0.25$ ($V_{\rm ac}=0.125\Gamma\approx T_K/2$). The dashed line shows the case of $\beta=0.5$ ($V_{\rm ac}=0.25\Gamma\approx T_K$) where the peak has been significantly reduced and the dot-dashed line shows the case of an intense signal where $\beta=0.75$ ($V_{\rm ac}=0.375\Gamma\approx 3T_K/2$). In this case the replicas of the Kondo become apparent (located at ω_0 and $-\omega_0$) and the peak at E_F has been strongly reduced. (c) corresponds to $\omega_0=\Gamma$: the solid line is for the case $\beta=0$; the dotted line shows the case $\beta=0.25$ ($V_{\rm ac}=0.25\Gamma\approx T_K$). At this ac intensity the first satellites of the Kondo resonance show up. The dashed line corresponds to $\beta=0.5$ ($V_{\rm ac}=0.5\Gamma\approx 2T_K$), in this case the time-averaged DOS at E_F has been suppressed below 0.5. The dot-dashed line corresponds to a very intense signal, $\beta=0.75$ ($V_{\rm ac}=0.75\Gamma\approx 3T_K$), the Kondo peak in this case has completely disappeared.

sponds to $\omega_0=\Gamma/4\approx T_K$ and different ac intensities $V_{\rm ac}\approx T_K/4$ ($\beta=0.25$), $V_{\rm ac}\approx T_K/2$ ($\beta=0.5$), and $V_{ac}\approx 3T_K/4$ ($\beta=0.75$). In all these situations the Kondo peak is slightly reduced, i.e., the dynamics of the correlated collective state is practically not influenced by the ac potential since both the ac frequency and the ac intensities are of the order of T_K. Furthermore, there is no evidence of replicas of the Kondo peak in the time-averaged DOS. By doubling ω_0 [Fig. 9(b)], the Kondo peak undergoes a stronger reduction as the absorption probability of photons rises by increasing β. However, a total suppression of the Kondo resonance is only reached for our largest ac frequency [Fig. 9(c), $\omega_0=\Gamma$]. Even for a small value of $\beta=0.25$, the Kondo resonance is reduced remarkably. For the highest ac amplitude ($\beta=0.75$) the Kondo resonance has been destroyed completely. The satellites become apparent in Figs. 9(b) and (c). In these cases both ω_0 and V_{ac} are much larger than the relevant energy scale of this problem given by T_K. In Fig. 9(c) even the second satellites are resolved at $\beta=0.5$. The satellites grow very slowly with β due to the two competing mechanisms previously discussed. This has to be compared with the so-called Tien-Gordon description where one expects an appreciable increase of the satellites in the time-averaged DOS as β increases.[42,43] More importantly, we point out that the Kondo satellites can only be observed by measuring the differential conductance $dI/dV_{\rm dc}|_{V_{\rm dc}=\omega_0}$. The finite dc voltage is an extra source of decoherence, i.e., reduction and broadening of the satellite peaks,[13,29] not addressed here. In the experimental results of Ref. 30 the sidepeaks never become apparent in the differential conductance. The experimental frequency range (10–50 GHz) corresponds, in our units, to a range from $\omega_0\approx\Gamma/5$ to $\omega_0\approx\Gamma$. For the lowest experimental ac frequency we do not observe satellites [Fig. 9(a)]. When $\omega_0\approx\Gamma$ [Figs. 9(c)] satellites are visible in the time-averaged DOS, although we stress again that these satellites can be masked in a differential conductance measurement inasmuch as the necessary dc bias voltage $V_{\rm dc}\approx\omega_0$ can be large enough to destroy the Kondo sidepeaks. Finally, we note that the mean-field resonances located at ϵ_0 and $\epsilon_0+U/2$ do not display satellites in the time-averaged DOS, since ω_0 is smaller than their widths which are of the order of 2Γ.

IV. SUMMARY

In conclusion, interesting features are found in the finite temperature transport ($T\ll T_K$) properties of QD's in the Kondo regime as an oscillatory gate voltage is applied. By solving the time-dependent Dyson equation we obtain the QD retarded Green's function and the time-averaged density of states within the framework of the Fermi-liquid theory. The interaction self-energy in our model is calculated, in the context of the Keldysh nonequilibrium technique, by perturbation theory up to second order in the on-site interaction and the effect of the ac potential is taken into account exactly for *all ranges of ac frequencies and ac intensities of the ac potential*. The Kondo resonance is modified by the external ac voltage in a different way depending on the range of ac frequencies studied. We find two different ac frequency ranges of opposite behavior, separated by a critical frequency ω_c where the linear conductance is minimum. ω_c depends on the ac intensity and moves to higher values as $V_{\rm ac}$ increases. At small ac frequencies, and fixed ac intensity, the Kondo peak decreases as ω_0 grows. Once the critical frequency is reached the opposite behavior is found and the Kondo peak increases as $\beta=V_{\rm ac}/\omega_0\to 0$. Our method, valid for arbitrary ac frequencies and ac intensities, finite on-site interaction and temperatures below T_K, complete the range of parameters previously studied.

ACKNOWLEDGMENTS

Work supported in part by the MEC of Spain under contracts PB96-0875, PB96-0085, and grant PF 98-07497938, by the NSF grant no. DMR 97-08499, and by the EU via contract FMRX-CT98-0180. We gratefully acknowledge discussions with David Sanchez and Silvano De Franceschi.

APPENDIX A: QD GREEN'S FUNCTIONS IN THE ABSENCE OF ac POTENTIAL

In this appendix, the QD Green's functions in the absence of time modulation are obtained. First of all, the QD Green's

function coupled to the leads is calculated, and afterwards the interaction in the Hartree approximation is included. A very simple calculation yields the exact lesser and greater Green's functions for H_{leads},

$$g_k^{<,(0)}(t-t') \equiv i\langle c_k^\dagger(t') c_k(t)\rangle = i f(\epsilon_k) e^{-i\epsilon_k(t-t')},$$
$$g_k^{>,(0)}(t-t') \equiv -i\langle c_k(t) c_k^\dagger(t')\rangle = -i[1-f(\epsilon_k)] e^{-i\epsilon_k(t-t')}, \tag{A1}$$

where $f(\epsilon_k)$ is the Fermi-Dirac distribution function. The lesser and greater hopping self-energies including hopping between the QD and the leads are written in terms of the previous Green's functions as,[39]

$$\Sigma_{sd}^{<}(t_1-t_2) = \sum_{k\in L,R} V_k^* g_k^{<}(t_1-t_2) V_k,$$
$$= i\sum_{L,R} \int \frac{d\epsilon}{2\pi} e^{-i\epsilon(t_1-t_2)} f_{L/R}(\epsilon)\Gamma^{L/R}(\epsilon), \tag{A2}$$

$$\Sigma_{sd}^{>}(t_1-t_2) = \sum_{k\in L,R} V_k^* g_k^{>}(t_1-t_2) V_k,$$
$$= -i\sum_{L,R} \int \frac{d\epsilon}{2\pi} e^{-i\epsilon(t_1-t_2)} \times [1-f_{L/R}(\epsilon)]\Gamma^{L/R}(\epsilon), \tag{A3}$$

where $\Gamma^L(\epsilon) = 2\pi\Sigma_{k\in L}|V_k|^2\delta(\epsilon-\epsilon_k)$ and a similar expression is obtained for $\Gamma^R(\epsilon)$. The retarded and advanced self-energies fulfill the relations

$$\Sigma_{sd}^{r}(t_1-t_2) = \theta(t_1-t_2)[\Sigma_{sd}^{>}(t_1-t_2) - \Sigma_{sd}^{<}(t_1-t_2)],$$
$$\Sigma_{sd}^{a}(t_1-t_2) = \theta(t_2-t_1)[\Sigma_{sd}^{<}(t_1-t_2) - \Sigma_{sd}^{>}(t_1-t_2)]. \tag{A4}$$

The Dyson equation for the retarded and advanced QD Green's functions is

$$g_{d,\sigma}^{r,a}(t-t') = g_{d,\sigma}^{r,a,(0)}(t-t') + \int dt_1 \int dt_2 g_{d,\sigma}^{r,a,(0)} \times (t-t_1)\Sigma_{sd}^{r,a}(t_1-t_2) g_{d,\sigma}^{r,a}(t_2-t'). \tag{A5}$$

Here $g_{d,\sigma}^{r,a,(0)}(t-t')$ are the QD Green's functions for H_{QD} [Eq. (3)] without the on-site repulsion term,

$$g_{d,\sigma}^{r,a,(0)}(t-t') = \mp i\,\theta(\pm t \mp t') e^{-i\epsilon_{0,\sigma}(t-t')}. \tag{A6}$$

In the absence of time dependence, it is advantageous to Fourier transform, getting

$$g_{d,\sigma}^{r,a}(\epsilon) = [(g_{d,\sigma(\epsilon)}^{r,a,(0)})^{-1} - \Sigma_{sd}^{r,a}(\epsilon)^{-1}, \tag{A7}$$

where

$$\Sigma_{sd}^{r,a}(\epsilon) = \sum_{k\in L,R} \frac{|V_k|^2}{\epsilon-\epsilon_k \pm i\eta} = \sum_{\alpha\in L,R} \Lambda_\alpha(\epsilon) \mp \frac{i}{2}\Gamma_\alpha(\epsilon). \tag{A8}$$

In the WB limit approximation the previous self-energies become $\Sigma_{sd}^{r,a}(\epsilon) = \mp\Sigma_{\alpha\in L,R}(i/2)\Gamma_\alpha$. By inserting these self-energies in Eq. (A7), the retarded and advanced QD Green's functions coupled to the leads are

$$g_{d,\sigma}^{r,a}(\epsilon) = \frac{1}{\epsilon-\epsilon_{0,\sigma} \pm \frac{i}{2}\sum_{\alpha\in L,R}\Gamma_\alpha}. \tag{A9}$$

One can Fourier transform back to get the time dependence of the retarded and advanced QD Green's functions,

$$g_{d,\sigma}^{r,a}(t,t') = \mp i\,\theta(\pm t \mp t') e^{-i\int_{t'}^{t} dt_1(\epsilon_{0,\sigma} \mp i\Sigma_{\alpha\in L,R}\Gamma_\alpha/2)}. \tag{A10}$$

Now the on-site interaction self-energy in the Hartree approximation is calculated via perturbation theory up to first order in U:

$$\Sigma_{d,\sigma}^{r,a(1)} = U n_{d,\bar{\sigma}}, \tag{A11}$$

where $n_{d,\bar{\sigma}} = \langle d_{\bar{\sigma}}^\dagger(t) d_{\bar{\sigma}}(t)\rangle$. By using the Dyson equation it is straightforward to get

$$\mathbf{g}_{d,\sigma}^{r,a}(t,t') = \mp i\,\theta(\pm t \mp t') e^{-i\int_{t'}^{t} dt_1(\epsilon_{0,\sigma} + U n_{d,\bar{\sigma}} \mp i\Sigma_{\alpha\in L,R}\Gamma_\alpha/2)}. \tag{A12}$$

APPENDIX B: QD GREEN'S FUNCTIONS IN THE PRESENCE OF ac POTENTIAL

In this appendix we derive analytical expressions for the lesser and greater QD Green's functions in the presence of an ac potential, including the coupling to the leads and the interaction in the Hartree approximation. As we mentioned in Sec. II, one needs to obtain these propagators in order to have an expression of the interaction self-energy which is given by Eq. (9). However, the lesser and greater QD Green's function are given as a function of the retarded and advanced self-energies [see Eq. (6)]. The Green's functions have the following expressions:[39]

$$G_{d,\sigma}^{r(a)}(t,t') = e^{-i(V_{\text{ac}}/\omega_0)\sin\omega_0 t} e^{i(V_{\text{ac}}/\omega_0)\sin\omega_0 t'} \mathbf{g}_{d,\sigma}^{r(a)}(t-t')$$
$$= \sum_{p=-\infty}^{p=\infty}\sum_{m=-\infty}^{m=\infty} J_m(\beta)J_p(\beta) e^{-ip\omega_0 t} e^{im\omega_0 t'} \mathbf{g}_{d,\sigma}^{r} \times (t-t'), \tag{B1}$$

where $J_m(\beta)$ is the Bessel function of order m and argument $\beta = V_{\text{ac}}/\omega_0$. The greater and lesser QD Green's functions are calculated by substituting the retarded and advanced QD Green's functions Eqs. (B1), in Eq. (6):

$$G^{<}_{d,\sigma}(t,t')=e^{-i(V_{\rm ac}\omega_0)\sin\omega_0 t}e^{i(V_{\rm ac}/\omega_0)\sin\omega_0 t'}\sum_{p=-\infty}^{p=\infty}\sum_{m=-\infty}^{m=\infty}J_m(\beta)J_p(\beta)\sum_{L,R}$$
$$\times\int_{-\infty}^{\infty}\frac{d\epsilon}{2\pi}\frac{e^{ip\omega_0 t}e^{-im\omega_0 t'}e^{-i\epsilon(t-t')}f_{L/R}(\epsilon)\Gamma^{L/R}(\epsilon)}{\left(\epsilon-p\omega_0-\bar{\epsilon}_{0,\sigma}+\frac{i}{2}\sum_{\alpha\in L,R}\Gamma_\alpha\right)\left(\epsilon-m\omega_0-\bar{\epsilon}_{0,\sigma}-\frac{i}{2}\sum_{\alpha\in L,R}\Gamma_\alpha\right)}, \tag{B2}$$

$$G^{>}_{d,\sigma}(t,t')=e^{-i(V_{\rm ac}/\omega_0)\sin\omega_0 t}e^{i(V_{\rm ac}/\omega_0)\sin\omega_0 t'}\sum_{p=-\infty}^{p=\infty}\sum_{m=-\infty}^{m=\infty}J_m(\beta)J_p(\beta)\sum_{L,R}$$
$$\times\int_{-\infty}^{\infty}\frac{d\epsilon}{2\pi}\frac{e^{ip\omega_0 t}e^{-im\omega_0 t'}e^{-i\epsilon(t-t')}[1-f_{L/R}(\epsilon)]\Gamma^{L/R}}{\left(\epsilon-p\omega_0-\bar{\epsilon}_{0,\sigma}+\frac{i}{2}\sum_{\alpha\in L,R}\Gamma_\alpha\right)\left(\epsilon-m\omega_0-\bar{\epsilon}_{0,\sigma}-\frac{i}{2}\sum_{\alpha\in L,R}\Gamma_\alpha\right)}, \tag{B3}$$

$$G^{<}_{d,\sigma}(t',t)=e^{i(V_{\rm ac}/\omega_0)\sin\omega_0 t}e^{-i(V_{\rm ac}/\omega_0)\sin\omega_0 t'}\sum_{p=-\infty}^{p=\infty}\sum_{m=-\infty}^{m=\infty}J_m(\beta)J_p(\beta)\sum_{L,R}$$
$$\times\int_{-\infty}^{\infty}\frac{d\epsilon}{2\pi}\frac{e^{-ip\omega_0 t}e^{im\omega_0 t'}e^{-i\epsilon(t'-t)}f_{L/R}(\epsilon)\Gamma^{L/R}}{\left(\epsilon-p\omega_0-\bar{\epsilon}_{0,\sigma}+\frac{i}{2}\sum_{\alpha\in L,R}\Gamma_\alpha\right)\left(\epsilon-m\omega_0-\bar{\epsilon}_{0,\sigma}-\frac{i}{2}\sum_{\alpha\in L,R}\Gamma_\alpha\right)}, \tag{B4}$$

$$G^{>}_{d,\sigma}(t',t)=e^{i(V_{\rm ac}/\omega_0)\sin\omega_0 t}e^{-i(V_{\rm ac}/\omega_0)\sin\omega_0 t'}\sum_{p=-\infty}^{p=\infty}\sum_{m=-\infty}^{m=\infty}J_m(\beta)J_p(\beta)\sum_{L,R}$$
$$\times\int_{-\infty}^{\infty}\frac{d\epsilon}{2\pi}\frac{e^{-ip\omega_0 t}e^{im\omega_0 t'}e^{-i\epsilon(t'-t)}[1-f_{L/R}(\epsilon)]\Gamma^{L/R}}{\left(\epsilon-p\omega_0-\bar{\epsilon}_{0,\sigma}+\frac{i}{2}\sum_{\alpha\in L,R}\Gamma_\alpha\right)\left(\epsilon-m\omega_0-\bar{\epsilon}_{0,\sigma}-\frac{i}{2}\sum_{\alpha\in L,R}\Gamma_\alpha\right)}. \tag{B5}$$

Once again we have taken $\bar{\epsilon}_{0,\sigma}=\epsilon_{0,\sigma}+Un_{d,\bar{\sigma}}$ being $n_{d,\bar{\sigma}}$ the QD averaged occupation. In the case of zero dc bias, the right and left Fermi-Dirac distribution functions are $f_{L,R}(\epsilon)=1/(e^{(\epsilon-E_F)/T}+1)$ where T is the temperature. The analytical expressions for the lesser and greater QD Green's function are obtained by integrating in the complex plane where the Fermi-Dirac distribution function can be written as a difference of two digamma functions which have poles in the lower and upper complex plane:

$$f(z)-\frac{1}{2}=-\frac{1}{2\pi i}\left[\psi\left(\frac{1}{2}+\frac{iz}{2\pi T}\right)-\psi\left(\frac{1}{2}-\frac{iz}{2\pi T}\right)\right]$$
$$=\sum_{k=0}^{k=\infty}\frac{1}{\frac{1}{2}+k-\frac{iz}{2\pi T}}-\frac{1}{\frac{1}{2}+k+\frac{iz}{2\pi T}}. \tag{B6}$$

The complex integrals are performed with the restriction $t-t'\geqslant 0$ because we use them to evaluate a retarded quantity [the retarded self-energy in Eq. (9)].

In order to abbreviate the notation, we define the following variables:

$$a_p=-\left(\bar{\epsilon}_{0,\sigma}+p\omega_0-\frac{i}{2}\sum_{\alpha\in L,R}\Gamma_\alpha\right),$$

$$b_m=-\left(\bar{\epsilon}_{0,\sigma}+m\omega_0+\frac{i}{2}\sum_{\alpha\in L,R}\Gamma_\alpha\right),$$

$$\alpha_p=\frac{1}{2}+\frac{i}{2\pi T}a_p,\quad \gamma_m=\frac{1}{2}+\frac{i}{2\pi T}b_m,\quad \zeta=e^{-2\pi T(t-t')},$$

$$\bar{u}_p=\frac{1}{2}\left[1-\tanh\left(\frac{1}{2T}a_p\right)\right],\quad \bar{v}_m=\frac{1}{2}\left[1-\tanh\left(\frac{1}{2T}b_m\right)\right]. \tag{B7}$$

With this notation, the analytic expressions for the lesser and greater QD Green's functions are

$$G^{>}(t,t') = e^{-i(V_{ac}/\omega_0)\sin\omega_0 t} e^{i(V_{ac}/\omega_0)\sin\omega_0 t'} \times \sum_{p=-\infty}^{p=\infty} \sum_{m=-\infty}^{m=\infty} J_m(\beta) J_p(\beta) \times \sum_{\alpha\in L,R} \frac{e^{ip\omega_0 t} e^{-im\omega_0 t'} \Gamma_\alpha}{(p-m)\omega_0 - i \sum_{\alpha\in L,R} \Gamma_\alpha} \times \left(\frac{F_1(\alpha_p,1,\alpha_p+1,\zeta)}{\alpha_p} - \frac{F_1(\gamma_m,1,\gamma_m+1,\zeta)}{\gamma_m} - 2\pi i(\overline{u_p}-1) e^{ia_p(t-t')} \right), \tag{B8}$$

$$G^{<}(t,t') = e^{-i(V_{ac}/\omega_0)\sin\omega_0 t} e^{i(V_{ac}/\omega_0)\sin\omega_0 t'} \times \sum_{p=-\infty}^{p=\infty} \sum_{m=-\infty}^{m=\infty} J_m(\beta) J_p(\beta) \times \sum_{\alpha\in L,R} \frac{e^{ip\omega_0 t} e^{-im\omega_0 t'} \Gamma_\alpha}{(p-m)\omega_0 - i \sum_{\alpha\in L,R} \Gamma_\alpha} \times \left(\frac{F_1(\alpha_p^*,1,\alpha_p^*+1,\zeta)}{\alpha_p^*} - \frac{F_1(\gamma_m^*,1,\gamma_m^*+1,\zeta)}{\gamma_m^*} - 2\pi i\, \overline{v_m} e^{-ib_m(t-t')} \right), \tag{B9}$$

$$G^{>}(t',t) = e^{i(V_{ac}/\omega_0)\sin\omega_0 t} e^{-i(V_{ac}\omega_0)\sin\omega_0 t'} \times \sum_{p=-\infty}^{p=\infty} \sum_{m=-\infty}^{m=\infty} J_m(\beta) J_p(\beta) \times \sum_{\alpha\in L,R} \frac{e^{-ip\omega_0 t} e^{im\omega_0 t'} \Gamma_\alpha}{(p-m)\omega_0 - i \sum_{\alpha\in L,R} \Gamma_\alpha} \times \left(\frac{F_1(\alpha_p,1,\alpha_p+1,\zeta)}{\alpha_p} - \frac{F_1(\gamma_m,1,\gamma_m+1,\zeta)}{\gamma_m} - 2\pi i\, \overline{u_p} e^{ia_p(t-t')} \right), \tag{B10}$$

$$G^{<}(t',t) = -e^{i(V_{ac}/\omega_0)\sin\omega_0 t} e^{-i(V_{ac}/\omega_0)\sin\omega_0 t'} \times \sum_{p=-\infty}^{p=\infty} \sum_{m=-\infty}^{m=\infty} J_m(\beta) J_p(\beta) \times \sum_{\alpha\in L,R} \frac{e^{-ip\omega_0 t} e^{im\omega_0 t'} \Gamma_\alpha}{(p-m)\omega_0 - i \sum_{\alpha\in L,R} \Gamma_\alpha} \times \left(\frac{F_1(\alpha_p^*,1,\alpha_p^*+1,\zeta)}{\alpha_p^*} - \frac{F_1(\gamma_m^*,1,\gamma_m^*+1,\zeta)}{\gamma_m^*} - 2\pi i(\overline{v_m}-1) e^{-ib_m(t-t')} \right). \tag{B11}$$

The functions F_1 are hypergeometric functions. Here γ^* and α^* are complex conjugates of γ and α, respectively. Once the greater and the lesser QD Green's functions are obtained, the retarded QD interaction self-energy is given by

$$\Sigma^{r,(2)}_{d,\sigma}(t,t') = -iU^2\theta(t-t')[G^{<}_{d,\sigma}(t,t')G^{>}_{\bar{d},\bar{\sigma}}(t',t)G^{<}_{\bar{d},\bar{\sigma}}(t,t') - G^{>}_{d,\sigma}(t,t')G^{<}_{\bar{d},\bar{\sigma}}(t',t)G^{>}_{\bar{d},\bar{\sigma}}(t,t')]. \tag{B12}$$

Here, we want to point out the nontrivial dependence of the retarded self-energy on the parameters of the ac voltage. With this nontrivial dependence the QD DOS strongly deviates from the usual single-particle Tien-Gordon behavior.[42,43]

[1] D. Goldhaber-Gordon, Hadas Shtrikman, D. Mahalu, David Abusch-Magder, V. Meirau, and M. Kostner, Nature (London) **391**, 156 (1998); D. Goldhaber-Gordon, J. Göres, M. A. Kastner, Hadas Shtrikman, D. Mahalu, and U. Meirau, Phys. Rev. Lett. **81**, 5225 (1998).

[2] S.M. Cronenwett, Tjerk H. Oosterkamp, and Leo. P. Kouwenhoven, Science **281**, 540 (1998).

[3] J. Schmid, J. Weis, K. Eberl, and K. von Klitzing, Physica B **256-258**, 182 (1998); Phys. Rev. Lett. **84**, 5824 (2000).

[4] A. C. Hewson, *The Kondo Problem to Heavy Fermions* (Cambridge University Press, Cambridge, 1993).

[5] D.C. Langreth, Phys. Rev. **150**, 516 (1966).

[6] T.K. Ng and P.A. Lee, Phys. Rev. Lett. **61**, 1768 (1988).

[7] L.I. Glazman and M.E. Raikh, Pis'ma. Zh. Éksp. Teor. Fiz. **47**, 378 (1988) [JETP Lett. **47**, 452 (1988)].

[8] A. Kawabata, J. Phys. Soc. Jpn. **60**, 3222 (1991).

[9] W. Van der Wiel, S. De Franceschi, T. Fujisawa, J. M. Elzerman, S. Tarucha, and L. P. Kouwenhoven, Science **289**, 2105 (2000).

[10] S. Hershfield, J.H. Davies, and J.W. Wilkins, Phys. Rev. Lett. **67**, 3720 (1991).

[11] A.L. Yeyati, A. Martín-Rodero, and F. Flores, Phys. Rev. Lett. **71**, 2991 (1993).

[12] Y. Meir, N.S. Wingreen, and P.A. Lee, Phys. Rev. Lett. **70**, 2601 (1993).

[13] N.S. Wingreen and Y. Meir, Phys. Rev. B **49**, 11 040 (1994).

[14] J. König, H. Schoeller, and Gerd Schön, Phys. Rev. Lett. **76**, 1715 (1996); Phys. Rev. B **54**, 16 820 (1996).

[15] P. Coleman, C. Hooley, and O. Parcollet, Phys. Rev. Lett. **86**, 4088 (2001).

[16] M. Plihal, D.C. Langreth, and Peter Nordlander, Phys. Rev. B **61**, R13 341 (2000); P. Coleman, C. Hooley, A. F. Ho, Y. Avishai, and Y. Boldin (unpublished).
[17] S. Sasaki, S. De Franceschi, J. M. Elzerman, W. G. van der Wiel, M. Eto, S. Tarucha, and L. P. Kouwenhoven, Nature (London) **405**, 764 (2000); M. Eto and Yu. V. Nazarov, Phys. Rev. Lett. **85**, 1306 (2000); M. Pustilnik, Y. Avishai, and K. Kikoin, *ibid.* **84**, 1756 (2000); D. Giuliano and A. Tagliacozzo, *ibid.* **84**, 4677 (2000); C. Tejedor and L. Martin-Moreno, Phys. Rev. B **63**, 035319 (2001).
[18] U. Gerland, J. von Delft, T. Costi, and Y. Oreg, Phys. Rev. Lett. **84**, 3710 (2000); Yang Ji, M. Heiblum, D. Sprinzak, D. Mahalu, and Hadas Shtrikman, Science **290**, 779 (2000).
[19] T. Ivanov, Europhys. Lett. **40**, 183 (1997); T. Pohjola, J. König, M. M. Salomaa, J. Schmid, H. Schoeller, and G. Schön, *ibid.* **40**, 189 (1997); T. Aono, M. Eto, and K. Kawamura, J. Phys. Soc. Jpn. **67**, 1860 (1998); A. Georges and Y. Meir, Phys. Rev. Lett. **82**, 3508 (1999); Natan Andrei, Gergely T. Zimanyi, and Gerd Schön, Phys. Rev. B **60**, R5125 (1999); Ramón Aguado and David C. Langreth, Phys. Rev. Lett. **85**, 1946 (2000); C.A. Büsser, E. V. Anda, A. L. Lima, Maria A. Davidovich, and G. Chiappe, Phys. Rev. B **62**, 9907 (2000); Wataru Izumida and Osamu Sakai, *ibid.* **62**, 10 260 (2000).
[20] L.P. Kouwenhoven, S. Jauhar, J. Orenstein, and P. L. McEven, Phys. Rev. Lett. **73**, 3443 (1994); T.H. Oosterkamp, L. P. Kouwenhoven, A. E. A. Koolen, N. C. van der Vaart, and J. P. M. Harmans, *ibid.* **78**, 1536 (1997).
[21] R.H. Blick, R. J. Haug, D. W. van der Weide, K. von Klitzing, and K. Ebere, Appl. Phys. Lett. **67**, 3924 (1995).
[22] C. Bruder and H. Schoeller, Phys. Rev. Lett. **72**, 1076 (1994).
[23] M.H. Hettler and H. Schoeller, Phys. Rev. Lett. **74**, 4907 (1995).
[24] T.K. Ng, Phys. Rev. Lett. **76**, 487 (1996).
[25] A. Schiller and S. Hershfield, Phys. Rev. Lett. **77**, 1821 (1996).
[26] P. Nordlander, Ned S. Wingreen, Yigal Meir, and David C. Langreth, Phys. Rev. B **61**, 2146 (2000).
[27] Rosa López, Ramón Aguado, Gloria Platero, and Carlos Tejedor, Phys. Rev. Lett. **81**, 4688 (1998).
[28] Y. Goldin and Y. Avishai, Phys. Rev. Lett. **81**, 5394 (1998); Phys. Rev. B **61**, 16 750 (2000).
[29] A. Kaminski, Yu. V. Nazarov, and L.I. Glazman, Phys. Rev. Lett. **83**, 384 (1999); Phys. Rev. B **62**, 8154 (2000).
[30] Jeroen M. Elzerman, S. De Franceschi, D. Goldhaber-Gordon, W. G. van der Wiel, and L. P. Kouwenhoven, J. Low Temp. Phys. **118**, 375 (2000).
[31] P. Nozieres, J. Low Temp. Phys. **17**, 31 (1974).
[32] A.M. Tsvelik and P.B. Wiegmann, Adv. Phys. **32**, 453 (1983).
[33] T.A. Costi and A.C. Hewson, J. Phys.: Condens. Matter **6**, 2519 (1994).
[34] R.M. Fye and J.E. Hirsch, Phys. Rev. B **38**, 433 (1988).
[35] Herbert Schoeller and Jürgen König, Phys. Rev. Lett. **84**, 3686 (2000).
[36] K. Yosida and K. Yamada, Suppl. Prog. Theor. Phys. **46**, 224 (1970).
[37] B. Horvatic and V. Zlatic, Solid State Commun. **54**, 957 (1985).
[38] L.V. Keldysh, Zh. Éksp. Teor. Fiz. **47**, 1515 (1964) [Sov. Phys. JETP **20**, 1018 (1965)].
[39] A.P. Jauho, N.S. Wingreen, and Y. Meir, Phys. Rev. B **50**, 5528 (1994).
[40] Peter Nordlander, Michael Pustilnik, Yigal Meir, Ned S. Wingreen, and David C. Langreth, Phys. Rev. Lett. **83**, 808 (1999).
[41] D. C. Langreth, in *Linear and Nonlinear Electron Transport in Solids*, Vol. 17 of *NATO Advanced Study Institute, Series B: Physics*, edited by J. T. Devreese and V. E. Van Doren (Plenum, New York, 1976), p. 3.
[42] P.K. Tien and J. Gordon, Phys. Rev. **129**, 647 (1963).
[43] Within the Tien and Gordon formalism (Ref. 42), the time-averaged DOS can be written as: $\Sigma_p J_p^2(\beta)\rho(\epsilon - p\omega_0)$, where $\rho(\epsilon - p\omega_0)$ is the static DOS evaluated at energies given by $\epsilon - p\omega_0$ (where p is an integer number). Thus the single-particle time-averaged DOS shows replicas of the main peaks located at $\epsilon_i \pm p\omega_0$ (ϵ_i being the position of the ith main resonance) with a spectral weight proportional to $J_p^2(\beta)$ and the main peaks have a spectral weight proportional to $J_0^2(\beta)$. This is in contradiction with our observation of a nontrivial dependence of the reduction of the Kondo resonance with β.